EFFECT OF POST-WELD HEAT TREATMENT ON TENSILE PROPERTIES OF FRICTION STIR-WELDED JOINTS OF NANOSTRUCTURED AA2024 ALLOY

Majid Naseri[1,2], Mohammad Alvand[3], Omid Imantalab[4], Davood Gholami[5], Ehsan Borhani[6]

[1]Department of Materials Engineering, Faculty of Engineering
Malayer University, Malayer, Iran, naserim@susu.ru (M.N.)
[2]South Ural State University, 76 Lenin Ave.
Chelyabinsk 454080, Russia
[3]Faculty of Materials and Metallurgical Engineering
Semnan University, Semnan, Iran, alvand_sut@yahoo.com (M.A.)
[4]Department of Materials Engineering, Faculty of Engineering
Bu-Ali Sina University, Hamedan, Iran, o.imantalab@basu.ac.ir (O.I.)
[5]School of Metallurgy and Materials Engineering
Iran University of Science and Technology, Tehran
Iran, davood_gholami@alumni.iust.ac.ir (D.G.)
[6]Department of Nanotechnology, Faculty of New Sciences and Technologies
Semnan University, Semnan, Iran, e.borhani@semnan.ac.ir (E.B.)

Received 05 December 2024
Accepted 10 April 2025
DOI: 10.59957/jctm.v60.i5.2025.10

ABSTRACT

Herein, the effect of post-weld heat treatment on the tensile properties of friction stir-welded (FSW) joints of nano/ultrafine-grained (NG/UFG) AA2024 alloy sheets produced by accumulative roll bonding (ARB) was investigated. Continuous and discontinuous dynamic recrystallizations were the main mechanisms of microstructure evolution in the stir zone of joints. As a result of recrystallization and larger grain sizes achieved during FSW, the ARB followed by FSW improved ductility and strain hardening. The ARB specimens had yield strength, tensile strength, and elongation values of 265 MPa, 450 MPa, and 7 %, respectively. FSW-welded ARB specimens showed yield strength, tensile strength, and elongation of 230 MPa, 440 MPa, and 11 %, respectively. After T6 treatment, there was an increase in tensile and yield strength of 550 and 310 MPa, respectively, due to the Orowan looping mechanism, which reduced the elongation of the specimen. In conclusion, FSW was suggested as a method of joining the NG/UFG AA2024 alloy sheets while highly retaining the refined microstructure.

Keywords: nanostructured materials, AA2024 alloy, friction stir welding, accumulative roll bonding, microstructure, mechanical properties.

INTRODUCTION

Many countries are recognizing the importance of reducing greenhouse gas emissions and fuel consumption in the aerospace and automotive industries. There is a growing effort to reduce the overall weight of vehicles in several industries, including automotive and aerospace [1, 2]. The demand for lower density materials has led to the replacement of high-strength steels and ferrous materials with Al and Mg alloys and metal matrix composites (MMCs). As a result of their low density and excellent mechanical strength, Al alloys are a suitable alternative to steel when it comes to reducing the overall weight of aerospace and automotive vehicles. As a result of this weight reduction, fuel consumption is reduced, and carbon dioxide emissions are reduced [3 - 7].

Applications of nano-grained (NG, 1 - 100 nm) and ultrafine-grained (UFG, 100 - 1000 nm) materials in

automotive and aerospace components have increased significantly in the last couple of decades for their high specific strength. Nowadays, several different severe plastic deformation (SPD) techniques, such as repeated folding and rolling (F&R), constrained groove pressing (CGP), repetitive corrugation and straightening (RCS), and accumulative roll bonding (ARB), have been developed to fabricate the bulk nanostructured sheets [8 - 14]. The invention of ARB by Saito et al. has attracted the attention of both the scientific and industrial communities due to its various advantages over other SPD processes [15, 16].

Metal sheet joining is a significant technological challenge, which adds an additional challenge to nanostructured Al sheets. Conventional fusion welding methods typically trigger the formation of intermetallic compounds and induce unfavourable microstructures and large distortions in the base metal [17 - 19]. To use nanostructured materials in structural applications, it is necessary to explore and understand their mechanical and microstructure properties of the welding process. Due to these characteristics, friction stir welding (FSW) can be used to join bulk nanostructured materials [20 - 22].

In spite of the fact that FSW has already been used to join hard-to-weld metals such as Mg and Al alloys, there has been little research regarding FSW of NG/UFG materials [23, 24]. Prior to the present study, the authors investigated the microstructure and texture of joined NG/UFG AA2024 alloy sheets produced by ARB and FSW [25, 26]. One reason for the different microstructure of the weld nugget was explained by the grain growth and softening phenomena. The present study completes our previous work by examining the tensile properties of the NG/UFG AA2024 alloy processed by ARB and FSW with and without T6 treatment. In this paper, the results of several conditions are discussed and compared. These are ARB, ARB + FSW, and ARB + FSW + T6.

EXPERIMENTAL

The material utilized in this research was a fully annealed commercial AA2024 alloy sheet (specifications are given in Table 1). Two strips of 150 mm × 50 mm × 0.8 mm were degreased with acetone and scratch brushed by a stainless-steel wire brush. Then, the prepared surfaces of the strips were placed on each other and fastened at both ends by steel wires. The assembly was cold rolled with an amount of reduction equal to 50 %. The rolled sheets were cut into two identical pieces, and the rolling was repeated for eight cycles. The detailed procedure of ARB was published elsewhere [27 - 29].

After eight ARB cycles, ARB-processed specimens were butt welded using the FSW machine. The welding tool made from a hot work tool steel (H13) was employed. The pin width and length were 6 mm and 0.6 mm, respectively, and the shoulder diameter was approximately 20 mm. The tilt angle of the tool was adjusted to 4°. FSW was performed at a traveling speed of 160 mm min^{-1} and a rotation speed of 250 rpm in the rolling direction. Also, a piece of the friction stir welded was further subjected to T6 treatment, i.e., solutionizing at 520°C for 2 h followed by artificial aging at 190°C for 5 h.

The microstructural studies were carried out using scanning transmission electron microscopy (STEM, JEOL JEM-2100F) and field emission scanning electron microscopy (FE-SEM, VEGA \\ TESCAN). For STEM characterization, the focused ion beam technique (FIB) Helios G4 Thermo Fisher Scientific apparatus was used.

Tensile tests were conducted using ISO 6892-01 for different cycles on the specimens. Tensile specimens had gauge widths and lengths of 5 mm and 10 mm, respectively. The tensile test was achieved on Hounsfield H50KS tensile testing equipment (Tinius Olsen Ltd, Redhill, UK) using an initial strain rate of 10^{-3} s^{-1}. Total elongation was calculated by subtracting gauge lengths

Table 1. Chemical composition of commercial AA2024 alloy sheet (in wt. %).

Ga	Cr	V	Ti	Zn	Si	Fe	Mn	Mg	Cu	Al
0.01	0.01	0.02	0.025	0.05	0.10	0.25	0.55	1.50	4.50	Bal.

before and after tensile testing. The tensile tests were performed on each specimen three times to ensure accuracy. The fracture surfaces of the tensile specimens were also examined by FE-SEM (VEGA \\ TESCAN).

RESULTS AND DISCUSSION

Fig. 1 demonstrates STEM micrographs from the rolling direction-normal direction (RD-ND) plane of the ARB-processed AA2024 alloy after the eighth cycle. As can be seen from Fig. 1, the grains in the RD are substantially elongated and have a high aspect ratio. The average lamellar boundary spacing along ND (thickness of the elongated grains) and the mean boundary spacing along RD (length of the elongated grains) are ~ 360 ± 10 nm and 845 ± 10 nm, respectively. As a result, a pancake-shaped lamellar ultrafine-grained microstructure is formed with a high density of dislocation substructures [15, 16, 30].

The back scattered electron SEM (BSE-SEM) image of the FSW-welded NG/UFG AA2024 alloy is illustrated in Fig. 2 shows. Four different areas can usually be differentiated after FSW: (i) base material, (ii) heat affected zone (HAZ), (iii) thermomechanical affected zone (TMAZ), and (iv) and stir zone or nugget, affected by the mechanical movement of the pin and the temperature increase [31, 32]. There is a clear reduction in grain size from the base material to the stir zone, confirmed by the SEM image. During the FSW process, the stir zone is subjected to high temperatures and intense plastic deformation, resulting in dynamic recrystallization and the creation of new grains with larger sizes than those seen in the ARB-processed specimen. The top region of the stir zone experiences higher temperatures and longer thermal cycles compared to the center of the stir zone. As a result, the grain size decreases from the top of the stir zone to the center, creating a gradient microstructure.

Based on the obtained results from Naseri et al., the microstructure of the TMAZ is highly redistributed and extended upward along the rotating tool axis, whereas the microstructure of the heat affected zone is more uniform [25]. The TMAZ experiences lower temperatures and plastic deformation compared to the stir zone, which is not enough for full recrystallization [33, 34]. Therefore, the microstructure in TMAZ remains distorted and the evidence of material shearing and flow in the upward direction around the rotating tool is obvious [25]. Due to frictional heat and plastic deformation caused by the rotating pin, the grain size in the TMAZ zone is still

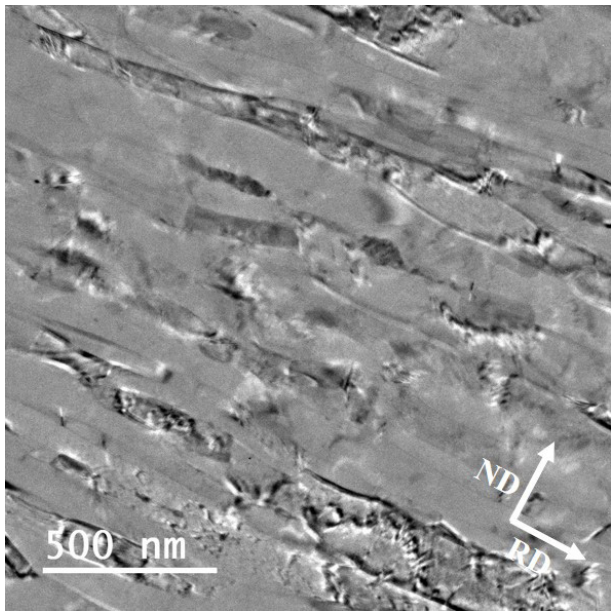

Fig. 1. STEM micrographs from RD–ND plane of AA2024 alloy after eight ARB cycles.

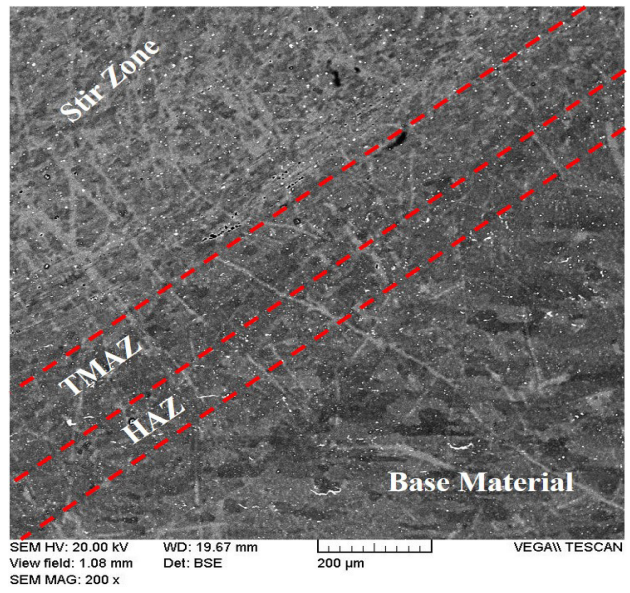

Fig. 2. BSE-SEM image of FSW-welded NG/UFG AA2024 alloy showing an overview of the four main areas.

larger than those not impacted by the welding process. Sato et al. observed pancake-shaped grains in the TMAZ and equiaxed and dynamically recrystallized grains in the NG/UFG AA1050 and NG/UFG AA1100 nuggets [33, 35].

Cabibbo et al. showed that different types of precipitation and complex patterns of precipitation occurred in different areas of the weld [36]. They found that precipitation coarsened and overaged in the TMAZ, and some precipitation dissolved in the stir zone. According to Borhani et al., pre-aging precipitates dissolve during the annealing of ARB-processed specimens [37]. Recently, it has been suggested by Cabibbo et al. that after FSW, precipitates may completely lose their strengthening function from over-aging, or they may dissolve into solution [36]. Additionally, according to some studies, dissolved precipitates may re-precipitate and increase the material's hardness [38, 39]. During FSW, precipitation and microstructural development in coarse-grained materials are complex, and they are even more difficult if the material has previously been processed by severe plastic deformation processes.

The engineering stress-strain curves of the annealed AA2024 alloy, ARB, ARB + FSW, and ARB + FSW + T6 specimens are shown in Fig. 3. Additionally, a summary of the specimens' yield strength (YS, evaluated by 0.2 % offset), elongation data, and ultimate tensile strength (UTS) are provided in Table 2. The YS and UTS of annealed AA2024 alloy are approximately 70 MPa and 190 MPa, respectively; the elongation is approximately 25 %. After eight cycles, the ARB-processed specimen's YS and UTS are, respectively, 265 MPa and 450 MPa, and its elongation is 7 %. Consequently, the YS and UTS increased by around 380 % and 240 %, respectively, because of the strengthening through grain refinement.

Regarding Fig. 3, the AA2024 alloys processed by ARB exhibit a lack of ductility and work hardening. Materials with nanocrystalline or ultrafine-grained structures generally cannot sustain uniform tensile elongation. According to several studies, strain hardening is virtually absent after a rapid hardening stage at low plastic strains (1 - 3 %), whereas coarse-grained polycrystalline metals exhibit strain hardening. Dislocation saturation or annihilation into grain boundaries causes nanocrystalline materials to have low strain hardening rates. This results in low strain hardening behaviour in SPD-processed materials [4, 40]. Because of low strain hardening, the material exhibits a low tensile ductility, as seen for the ARB-processed AA2024 alloy.

Contrary to ARB, FSW followed by ARB (ARB + FSW specimen) exhibits improved ductility and strain hardening, likely due to recrystallization and larger grain sizes achieved during FSW. With ARB+FSW, the specimen exhibited YS, UTS, and elongation of

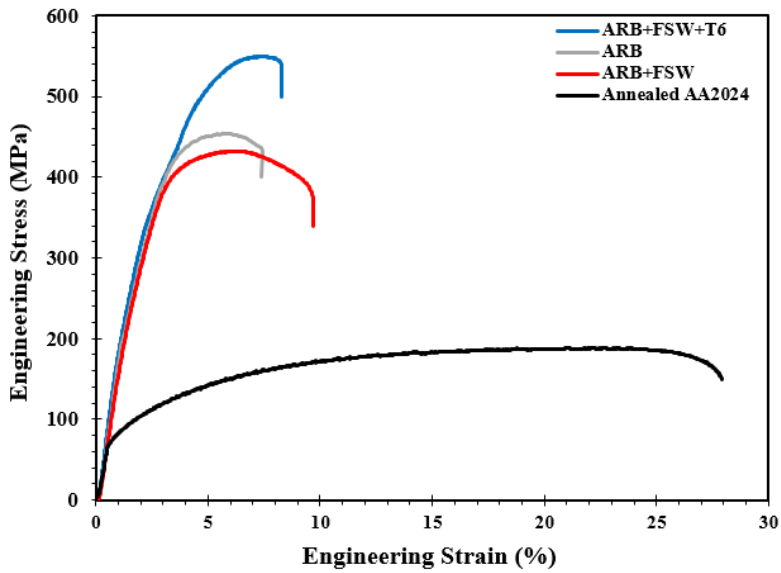

Fig. 3. Typical Engineering stress-strain curves of the annealed AA2024, ARB, ARB + FSW, and ARB + FSW + T6 specimens.

230 MPa, 440 MPa, and 11 %, respectively, compared with the ARB-processed specimen (265 MPa, 450 MPa, and 7 %). With a bimodal grain structure across the weld, the welded specimen demonstrated an attractive balance between strength and elongation. Moreover, a T6 treatment could further improve the YS (310 MPa) and UTS (550 MPa) of the welded joint, while its ductility significantly decreased. Due to the formation of nano-sized precipitates, the material's strength can be improved through the Orowan looping mechanism [37, 41]. Furthermore, nano-sized particles provide stress concentration and can act as nucleation sites for voids, which reduce the ductility of the material under the T6 conditions [37].

Fig. 4 shows the fracture surfaces after the tensile test of the annealed AA2024, ARB, ARB + FSW, and

Table 2. Experimental and calculated values of offset yield strength, tensile strength, and elongation for the specimens.

Specimen	Yield Strength, MPa	Tensile Strength, MPa	Elongation, %
Annealed AA2024	70	190	25
ARB	265	450	7
ARB + FSW	230	440	11
ARB + FSW + T6	310	550	8

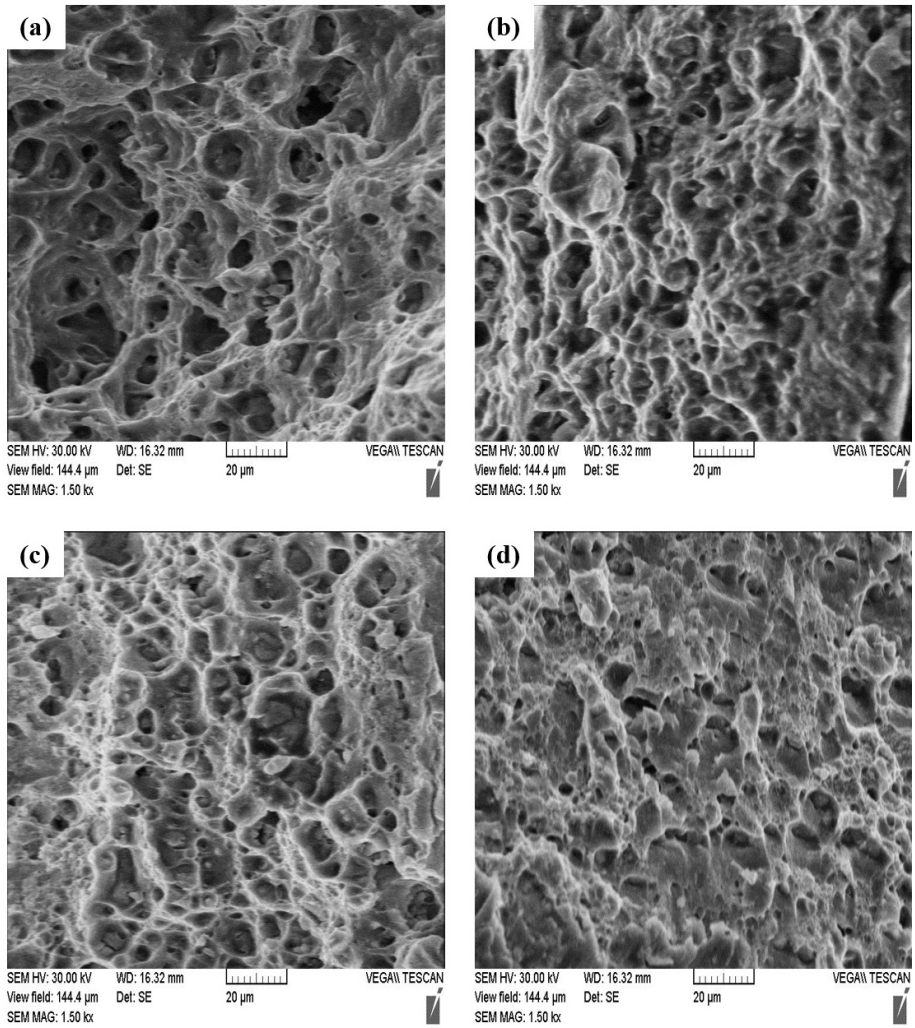

Fig. 4. SEM micrographs of the fracture surfaces after tensile test for: (a) annealed AA2024; (b) ARB; (c) ARB + FSW and (d) ARB + FSW + T6 specimens.

ARB + FSW + T6 specimens. The fracture surface is characterized by void formation, growth, and coalescence, all signs of ductile fracture [42]. There are pores on the fracture surface that serve as previous voids and encourage further damage. Here, the fracture is caused by both the casting porosities and the voids created by FSW. Despite this, all specimens exhibit ductile fractures, which are evaluated by dimples and a fibrous appearance. The annealed AA2024 alloy specimen exhibits deep, evenly spaced dimples as shown in Fig. 4a. After eight ARB cycles (Fig. 4b), thin and elongated dimples are observed to some extent. These characteristics are the evidence of low strain hardening and low elongation in the ARB-processed specimens [43, 44]. There are fine populated dimples on the fracture surface of the FSW joints (Figs. 4c and d). In contrast, the fracture surfaces of the ARB + FSW + T6 specimen have fewer dimples than the ARB + FSW specimen, which is consistent with the tensile test outcomes. Dimples are oriented toward the loading direction, suggesting that FSW joints fail predominantly in the ductile fracture mode.

Due to the brittle nature of welded Al alloys, fusion-based welding cannot be successful when combining Al components. Solid-state processes can be used to join unwearable Al alloys by heating the workpiece below the melting point of the base alloy. Friction stir welding has been extensively researched for joining and treating solid-state alloys of comparable and different grades. From the results of this work, FSW appears to be a solid-state welding technique that can be used to join or assemble the challenging NG/UFG AA2024 alloys. Therefore, concurrent improvement in ductility and strength can be achieved by optimizing heat treatment and employing different approaches.

CONCLUSIONS

The effect of post-weld heat treatment on the tensile properties of friction stir-welded (FSW) joints of nano/ultrafine-grained (NG/UFG) AA2024 alloy sheets produced by accumulative roll bonding (ARB) was investigated. It is confirmed that ARB is the suitable process for the fabrication of nanostructured material sheets, and the NG/UFG microstructure can be highly retained within the stir zone after friction-based solid-state welding. However, the grain size slightly increases after FSW welding due to dynamic recrystallization. In the nugget zone, grains are equiaxed and homogeneous. The ARB-welded specimens have 230 MPa yield stress, 440 MPa tensile strength, and 11 % elongation compared to ARB-processed specimens with 265 MPa yield stress, 450 MPa tensile strength, and 7 % elongation. The T6 treatment also increases the joint's yield strength and tensile strength to 310 MPa and 550 MPa, respectively, while reducing elongation to 8 %. All specimens have dimples on their fracture surfaces, which is typical for the ductile fracture mode. Finally, FSW is suggested as a method of joining the NG/UFG AA2024 alloy sheets while highly retaining the refined microstructure.

***Authors' contributions**: M.N: Conceptualization, Investigation, Validation, Writing-Original Draft, Writing-Review and Editing; M.A.: Conceptualization, Investigation, Validation; O.I.: Writing-Original Draft, Writing-Review and Editing; D.G.: Writing-Review & Editing. E.B.: Writing-Review & Editing.*

REFERENCES

1. P.E. Sikorska, The need for legal regulation of global emissions from the aviation industry in the context of emerging aerospace vehicles, International Comparative Jurisprudence, 1, 2, 2015, 133-142.
2. Z. Liu, Y. Geng, M. Adams, L. Dong, L. Sun, J. Zhao, H. Dong, J. Wu, X. Tian, Uncovering driving forces on greenhouse gas emissions in China' aluminum industry from the perspective of life cycle analysis, Applied Energy, 166, 2016, 253-263.
3. M. Naseri, A. Hassani, M. Tajally, An alternative method for manufacturing Al/B_4C/SiC hybrid composite strips by cross accumulative roll bonding (CARB) process, Ceramics International, 41,10, 2015, 13461-13469.
4. M. Naseri, M. Reihanian, E. Borhani, A new strategy to simultaneous increase in the strength and ductility of AA2024 alloy via accumulative roll bonding (ARB), Materials Science and Engineering: A, 656, 2016, 12-20.
5. R. Jamaati, M. Naseri, M.R. Toroghinejad, Wear behavior of nanostructured Al/Al_2O_3 composite fabricated via accumulative roll bonding (ARB) process, Materials and Design, 59, 2014, 540-549.
6. H.Y. Diao, R. Feng, K.A. Dahmen, P.K. Liaw, Fundamental deformation behavior in high-entropy

alloys: An overview, Current Opinion in Solid State and Materials Science, 21, 5, 2017, 252-266.
7. M. Naseri, A.O. Moghadam, M. Anandkumar, S. Sudarsan, E. Bodrov, M. Samodurova, E. Trofimov, Enhancing the mechanical properties of high-entropy alloys through severe plastic deformation: A review, Journal of Alloys and Metallurgical Systems, 5, 2024, 100054.
8. R.Z. Valiev, A.P. Zhilyaev, T.G. Langdon, Bulk Nanostructured Materials: Fundamentals and Applications, Wiley, 2013.
9. N. Hansen, X. Huang, R. Ueji, N. Tsuji, Structure and strength after large strain deformation, Materials Science and Engineering: A, 387-389, 2004, 191-194.
10. R.Z. Valiev, R.K. Islamgaliev, I.V. Alexandrov, Bulk nanostructured materials from severe plastic deformation, Progress in Materials Science, 45, 2, 2000, 103-189.
11. A.K. Gupta, T.S. Maddukuri, S.K. Singh, Constrained groove pressing for sheet metal processing, Progress in Materials Science, 84, 2016, 403-462.
12. A. Keyvani, M. Naseri, O. Imantalab, D. Gholami, K. Babaei, A. Fattah-alhosseini, Microstructural characterization and electrochemical behavior of nano/ultrafine grained pure copper through constrained groove pressing (CGP), Journal of Materials Research and Technology, 11, 2021, 1918-1931.
13. S. Hashemipour, A. Eivani, H. Jafarian, M. Naseri, N. Park, Microstructure and mechanical properties development of nano/ultrafine grained AISI 316L austenitic stainless steel prepared by repetitive corrugation and straightening by rolling (RCSR), Materials Research Express, 5, 12, 2018, 126519.
14. M. Naseri, A.O. Moghaddam, N. Shaburova, D. Mikhailov, D. Gholami, A.H.I. Mourad, A. Pellenen, E. Trofimov, Upgrading the strength-ductility trade-off and wear resistance of $Al_{0.25}CoCrFeNiCu$ and $Al_{0.45}CoCrFeNiSi_{0.45}$ high-entropy alloys through severe cold rolling process, Materials Today Communications, 38, 2024, 108036.
15. Y. Saito, N. Tsuji, H. Utsunomiya, T. Sakai, R.G. Hong, Ultra-fine grained bulk aluminum produced by accumulative roll-bonding (ARB) process, Scripta Materialia, 39, 9, 1998, 1221-1227.
16. Y. Saito, H. Utsunomiya, N. Tsuji, T. Sakai, Novel ultra-high straining process for bulk materials-development of the accumulative roll-bonding (ARB) process, Acta Materialia, 47, 2, 1999, 579-583.
17. H. Li, J. Zou, J. Yao, H. Peng, The effect of TIG welding techniques on microstructure, properties and porosity of the welded joint of 2219 aluminum alloy, Journal of Alloys and Compounds, 727, 2017, 531-539.
18. P. Praveen, P.K.D.V. Yarlagadda, Meeting challenges in welding of aluminum alloys through pulse gas metal arc welding, Journal of Materials Processing Technology, 164-165, 2005, 1106-1112.
19. M. Haghshenas, A.P. Gerlich, Joining of automotive sheet materials by friction-based welding methods: A review, Engineering Science and Technology, an International Journal, 21, 1, 2018, 130-148.
20. R.S. Mishra, Z.Y. Ma, Friction stir welding and processing, Materials Science and Engineering: R: Reports, 50, 1-2, 2005, 1-78.
21. C.J. Dawes, W.M. Thomas, Friction stir joining of aluminum alloys, TWI Bulletin, The Welding Institute, 1995, 124-127.
22. G. Cam, Friction stir welded structural materials: Beyond Al-alloys, International Materials Reviews, 56, 1, 2011, 1-48.
23. Y.S. Sato, M. Urata, Y. Kurihara, S. Park, H. Kokawa, K. Ikeda, N. Tsuji, Microstructural evolution during friction stir welding of ultrafine grained Al alloys, Materials Science Forum, 2006, 169-174.
24. A. Fattah-alhosseini, M. Naseri, D. Gholami, O. Imantalab, F. Attarzadeh, M. Keshavarz, Microstructure and corrosion characterization of the nugget region in dissimilar friction-stir-welded AA5083 and AA1050, Journal of Materials Science, 54, 2019, 777-790.
25. M. Naseri, M. Alvand, D. Gholami, E. Borhani, H. Abdollah-Pour, S. Fakhravar, Friction stir welding of nano/ultrafine-grained AA2024 alloy produced through an accumulative roll bonding process, MRS Communications, 12, 1, 2022, 51-57.
26. M. Naseri, M. Alvand, E. Ahmadi, S. Hosseini, D. Gholami, A.H.I. Mourad, E. Borhani, Effect of cube texture on local softening of friction stir welded joints for nanostructured AA2024 processed by accumulative roll bonding, Journal of Materials Research and Technology, 28, 2024, 3507-3513.

27. M. Alvand, M. Naseri, E. Borhani, H. Abdollah-Pour, Nano/ultrafine grained AA2024 alloy processed by accumulative roll bonding: A study of microstructure, deformation texture and mechanical properties, J. Alloys Compd, 712, 2017, 517-525.
28. M. Naseri, E. Borhani, O. Imantalab, H.W. Jang, M. Shokouhimehr, A. Fattah-alhosseini, Correlation between crystallographic texture and electrochemical behavior of nano/ultrafine-grained AA2024 alloy processed by accumulative roll bonding process, Journal of Materials Research and Technology, 18, 2022, 4256-4266.
29. M. Naseri, M. Reihanian, E. Borhani, Effect of strain path on microstructure, deformation texture and mechanical properties of nano/ultrafine grained AA1050 processed by accumulative roll bonding (ARB), Materials Science and Engineering: A, 673, 2016, 288-298.
30. M. Naseri, A.O. Moghaddam, N. Shaburova, D. Gholami, A. Pellenen, E. Trofimov, Ultrafine lamellar microstructures for enhancing strength-ductility synergy in high-entropy alloys via severe cold rolling process, Journal of Alloys and Compounds, 965, 2023, 171385.
31. I. Sabry, V.P. Singh, M. Alkhedher, N.E. El-Zathry, A.-H.I. Mourad, M. Naseri, Effect of rotational speed and penetration depth on Al-Mg-Si welded T-joints through underwater and conventional friction stir welding, Journal of Advanced Joining Processes, 9, 2024, 100207.
32. M. Alvand, M. Naseri, E. Borhani, H. Abdollah-Pour, Microstructure and crystallographic texture characterization of friction stir welded thin AA2024 Aluminum alloy, Iranian Journal of Materials Science cf. Engineering, 15, 1, 2018, 3-63.
33. Y.S. Sato, Y. Kurihara, S.H.C. Park, H. Kokawa, N. Tsuji, Friction stir welding of ultrafine grained Al alloy 1100 produced by accumulative roll-bonding, Scripta Materialia, 50, 1, 2004, 57-60.
34. H. Mirzadeh, Grain refinement of magnesium alloys by dynamic recrystallization (DRX): A review, Journal of Materials Research and Technology, 25, 2023, 7050-7077.
35. Y.S. Sato, M. Urata, Y. Kurihara, S.H.C. Park, H. Kokawa, K. Ikeda, N. Tsuji, Microstructural Evolution during Friction Stir Welding of Ultrafine Grained Al Alloys, Materials Science Forum, 503-504, 2006, 169-174.
36. M. Cabibbo, H.J. McQueen, E. Evangelista, S. Spigarelli, M. Di Paola, A. Falchero, Microstructure and mechanical property studies of AA6056 friction stir welded plate, Materials Science and Engineering: A, 460-461, 2007, 86-94.
37. E. Borhani, H. Jafarian, D. Terada, H. Adachi, N. Tsuji, Microstructural Evolution during ARB Process of Al-0.2 mass% Sc Alloy Containing Al_3Sc Precipitates in Starting Structures, Materials Transactions, 53, 1, 2012, 72-80.
38. J.Q. Su, T.W. Nelson, R. Mishra, M. Mahoney, Microstructural investigation of friction stir welded 7050-T651 aluminium, Acta Materialia, 51, 3, 2003, 713-729.
39. H. Qin, H. Zhang, H. Wu, The evolution of precipitation and microstructure in friction stir welded 2195-T8 Al–Li alloy, Materials Science and Engineering: A, 626, 2015, 322-329.
40. M.A. Meyers, A. Mishra, D.J. Benson, Mechanical properties of nanocrystalline materials, Progress in Materials Science, 51, 4, 2006, 427-556.
41. Z. Zhang, D.L. Chen, Contribution of Orowan strengthening effect in particulate-reinforced metal matrix nanocomposites, Materials Science and Engineering: A, 483-484, 2008, 148-152.
42. T.H. Courtney, Mechanical Behavior of Materials, McGraw Hill Custom Pub, 2000.
43. M. Reihanian, M. Naseri, M. Jalili Shahmansouri, Effect of the particle size on the deformation and fracture behavior of Al/4vol.% Al_2O_3 composite produced by accumulative roll bonding (ARB), Iranian Journal of Materials Forming, 2, 2, 2015, 14-26.
44. M. Naseri, M. Reihanian, E. Borhani, EBSD characterization of nano/ultrafine structured Al/Brass composite produced by severe plastic deformation, Journal of Ultrafine Grained and Nanostructured Materials, 51, 2, 2018, 123-138.